

Generation of high-order harmonic continuum with two-hump-structure infrared laser pulse

Candong Liu (刘灿东)¹, Pengfei Wei (尉鹏飞)^{2*}, Jing Miao (苗 境)¹,
Chunmei Zhang (张春梅)¹, Yansui Huang (黄延穗)¹, Yinghui Zheng (郑颖辉)¹,
Yuxin Leng (冷雨欣)¹, and Zhinan Zeng (曾志男)^{1**}

¹State Key Laboratory of High Field Laser Physics, Shanghai Institute of Optics and Fine Mechanics,
Chinese Academy of Sciences, Shanghai 201800, China

²College of Physics and Electronic Information Engineering,
Wenzhou University, Wenzhou 325035, China

*Corresponding author: pfw@wzu.edu.cn; **corresponding author: zhinan_zeng@mail.siom.ac.cn

Received October 28, 2013; accepted January 15, 2014; posted online February 28, 2014

We experimentally investigate the high-order harmonic generation in argon gas cell driven by a multi-cycle broadband infrared laser pulse from a tunable optical-parametric-amplifier (OPA) source. The generation of high-order harmonic continuum with the cut-off photon energy up to 110 eV is observed by tuning the chirp of the 800-nm laser pulse which pumps OPA source. The generation of harmonic continuum is understood in terms of the two-hump structure of the OPA output spectrum and the optimal relative phase of the two humps. The demonstrated scheme is of importance for the generation of extreme ultraviolet (XUV) continuum at higher photon energy region.

OCIS codes: 020.2649, 190.2620, 190.4410.

doi: 10.3788/COL201412.030201.

High-order harmonic generation (HHG) has been intensively explored in the past decade, since it is a promising approach for table-top extreme ultraviolet (XUV) light sources and attosecond ultrafast pulse^[1–7]. The underlying dynamics of HHG has been widely and deeply studied, and harmonic generation process is usually described by classical three-step model, strong-field approximate and Feynman's path-integral approach^[8–10]. Both theoretical and experimental results demonstrate that either the enhancement of the laser intensity or the use of the longer wavelength can extend the cut-off photon energy. Yakovlev *et al.*^[11] theoretically predicted several important advantages when using mid-infrared driving laser pulse. One of these advantages is that an isolated attosecond pulse with photo energy above 100 eV can be extracted from plateau harmonics. Lan *et al.*^[12] also theoretically showed that the harmonic yield can be enhanced and scales as $\lambda^{-3} - \lambda^{-4}$ in the plateau region by the two-color infrared laser fields, which falls more slowly as the increase of the driving laser wavelength compared with $\lambda^{-5} - \lambda^{-6}$ in a one-color infrared field. Therefore, the two-color scheme has been demonstrated as an effective way to achieve an enhancement of the high harmonics^[13], and has also proved to be a new insight into atomic and molecular orbital imaging or transient dynamic^[14–16]. By combining the fundamental 800-nm laser pulse and another infrared 1.3–1.6- μm parametric pulse, Vozzi *et al.*^[17] reported the generation of a coherent continuous spectrum above 100 eV, and Takahashi *et al.*^[18] also achieved the very intense attosecond pulse generation through optimizing such multi-cycle two-color laser field. Moreover, by combining two noncommensurate infrared laser pulses, Negro *et al.*^[19] experimentally demonstrated a new technique for the temporal gating

of high-order harmonic continuum.

In this letter, we demonstrate the generation of the XUV continuum beyond 110 eV using only one multi-cycle optical-parametric-amplifier (OPA) laser pulse with the passively stabilized carrier-envelope-phase (CEP). Through changing the chirp of OPA pump pulse and the crystal phase-matching angle, the OPA output is optimized to exhibit the broadband spectrum with the two-hump structure, which allows for the generation of the more continuous high harmonic spectrum. This is different from the traditional two-color scheme where the delay line of the two pulses is optimized. We also experimentally investigate the relationship between the two-hump distance of OPA spectrum and the degree of the variation of harmonic spectrum from the discrete to the continuous.

In the experiment, the home-built infrared OPA system^[20–22] is driven by a commercial Ti: Sapphire laser source operating at 800-nm wavelength and 45-fs pulse duration with a repetition rate of 1 kHz. The laser pulse of 6.8-mJ energy is used to pump the OPA source, generating the CEP stabilized output pulse tunable from 1.6 to 1.9 μm with the pulse energy about 1.2 mJ and the pulse duration about 48 fs. High-order harmonics are generated by focusing the infrared pulses in argon gas cell located in a high-vacuum interaction chamber. The laser intensity in the interaction region is estimated to about 1.5×10^{14} W/cm². The gas cell with a stagnation pressure of about 100 Torr is 2-mm long. The harmonic emission is detected by a home-made flat-field soft X-ray grating spectrograph, which consists of a gold-coated spherical mirror, a gold-coated cylindrical mirror, a slit, a Hitachi flat-field grating (1200 grooves/mm) and a soft x-ray CCD (SX 400, Princeton Instruments, USA).

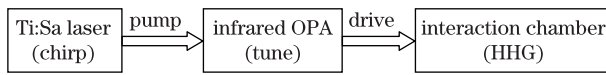


Fig. 1. Experimental setup.

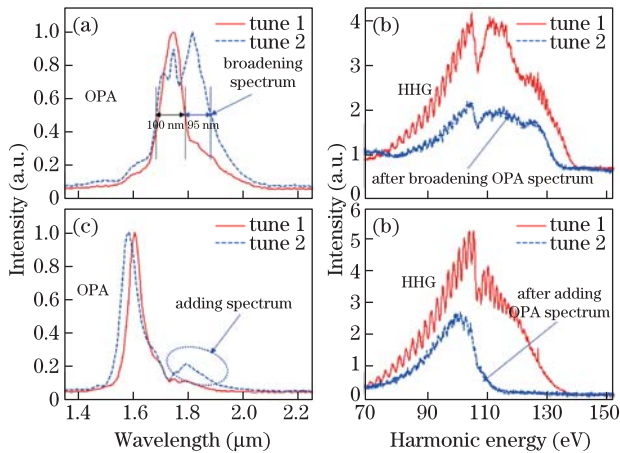


Fig. 2. (Color online) (a) OPA spectra with two different bandwidths (FWHM is from 100 to 195 nm), and (b) the corresponding HHG spectra before and after broadening OPA spectrum. (c) OPA spectra with and without the superposition of a weak spectrum component (One is the main component at the central wavelength of $1.6 \mu\text{m}$ and the other is the weak component at the central wavelength of $1.8 \mu\text{m}$), and (d) the corresponding HHG spectra before and after adding OPA spectrum.

A 500-nm-thick zirconium foil is placed at the entrance of the spectrograph in order to block the infrared driving pulse. The spectrometer is set to observe the spectral range between 70 and 155 eV. The experimental setup is shown in Fig. 1.

The bandwidth and central wavelength of the OPA output can be controlled by adjusting the seed input and the crystal phase-matching angle. We firstly measure separately the HHG spectrum for the OPA output operating at a central wavelength of $1.75 \mu\text{m}$ in the case of the narrower-band and broader-band phase-matching conditions. Figure 2(a) shows the spectrum intensity of the OPA output for the two phase-matching conditions, which corresponds to the bandwidth (full-width at half-maximum, FWHM) tunable from 100 to 195 nm. The generated high harmonic spectrum for the two cases is shown in Fig. 2(b). We also measure the HHG spectrum for the OPA output operating at the central wavelength of $1.6 \mu\text{m}$ with and without the superposition of the relatively weak spectrum component centered at the wavelength of $1.8 \mu\text{m}$. The OPA output spectrum and the correspondingly generated high harmonic spectrum for the two cases are shown in Figs. 2(c) and (d), respectively. Obviously, the extension of the OPA spectrum bandwidth or the inclusion of the weak spectrum component by tuning the OPA system is in favor of the generation of high harmonic continuum. Especially for the latter such phenomena are more evident. Furthermore, from the comparison between the blue-dashed line and the red-solid line in both Figs. 2(b) and (d), one can see that the HHG spectra are characterized by the weaker intensities and the lower cutoff energies in the case of broadening and adding the OPA spectrum, which can be attributed to the reduced conversion efficiency when

operating the OPA system near the degenerate condition associated with the broader-band phase matching. Additionally, Figs. 2(b) and (d) show that there is a dip around 105 eV in the HHG spectrum. It is possibly caused by nodal point in the modulus of the radial wave function of Ar 3p subshell in momentum space, as represented in Ref. [23].

We point out that both broadening the OPA spectrum and introducing the additional spectrum component make the spectrum profile exhibit the two-hump structure. In order to further investigate how the two-hump structure affects the variation of high harmonic spectrum from the discrete to the continuous, we measure the HHG spectrum with different two-hump distances by slightly changing the chirp parameter of the 800-nm OPA pump pulse, which can be achieved by tuning the grating separation in the pulse compressor of the Ti: sapphire laser source while keeping the pulse energy, the pulse duration and the spectral profile of the OPA output almost identical. Figure 3(a) shows the OPA output spectrum, exhibiting the two-hump distance of 40 nm, in the case of the two chirp values of pump pulse, denoted by chirp 1 (red-solid line) and chirp 2 (blue-dashed line). Figure 3(b) shows the corresponding HHG spectra with the discrete structure (red-solid line) for chirp 1 and the continuous structure (blue-dashed line) for chirp 2. We can see that the degree of the variation from the discrete to the continuous is not very evident due to the small two-hump distance. In contrast, we try to increase the two-hump distance by tuning the OPA system to a new working status. Figure 3(c) shows the OPA output spectra of the 200-nm two-hump distance produced by two different pump chirps, and Fig. 3(d) shows the correspondingly discrete and continuous HHG spectra. We can see that the large two-hump distance can lead to the much more evident variation of the harmonic spectrum from the discrete to the continuous. Therefore, the two-hump distance of the OPA spectrum plays an important role in the degree of the variation of the generated harmonic spectrum from the discrete to the continuous.

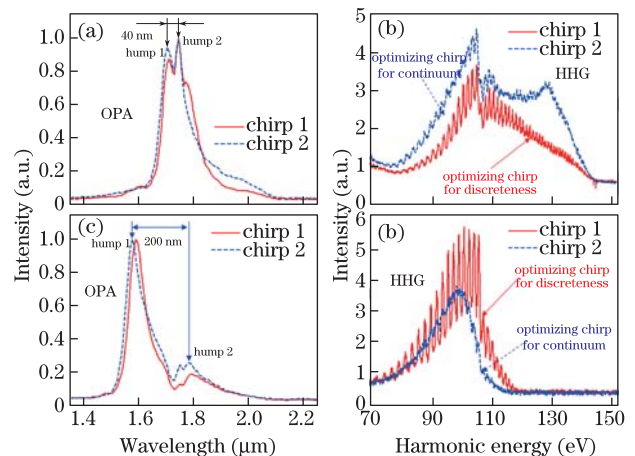


Fig. 3. (Color online) (a) OPA spectra with the 40-nm two-hump distance produced by the two different pump chirps and (b) the discrete and the continuous HHG spectra separately corresponding to the two chirps. (c) OPA spectra with the 200-nm two-hump distance produced by another two different pump chirps and (d) the discrete and the continuous HHG spectra separately corresponding to the two chirps.

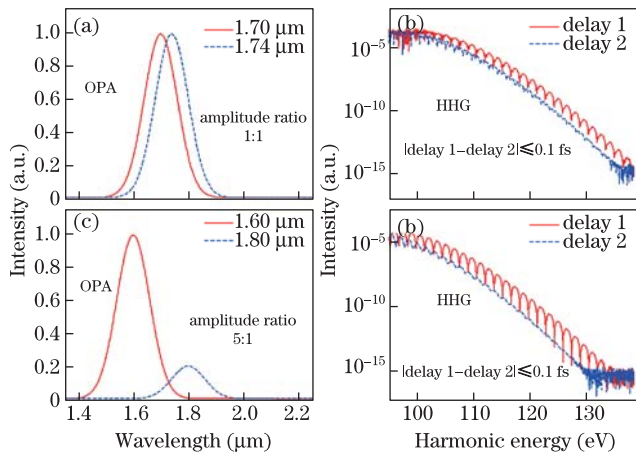


Fig. 4. (Color online) (a) OPA spectra in the simulation with the central wavelengths of 1.70 and 1.74 μm , and (b) the corresponding HHG spectra after optimizing the time delay for discreteness and continuum. (c) OPA spectra in the simulation with the central wavelengths of 1.60 and 1.80 μm , and (d) the corresponding HHG spectra after optimizing the time delay for discreteness and continuum.

The previous two-color scheme enable the generation of the high-order harmonic continuum through the superposition of the two adjacent noncommensurate infrared laser pulses from OPAs^[19,20]. For example, in Negro's experiment, the two infrared pulses were at the central wavelengths of 1.35 and 1.75 μm and the full bandwidth of each color component was about 300 nm. In our scheme, the XUV quasi-continua with photon energy above 110 eV can be generated using only one infrared laser pulse with the two-hump spectrum structure, due to the fact that the full bandwidth of our infrared pulse is relatively broader. Here the spectrum range mainly covers from 1.5 to 2.0 μm at two central wavelengths of 1.6 and 1.8 μm and each hump has the relative bandwidth about 250 nm. In comparison with the previous two-color scheme where the HHG spectrum from the discrete to the continuous can be controlled by the superposition of two laser pulses, we achieve the HHG spectrum from the discrete to the continuous by optimizing the pump chirp, which alters the relative phase between the two humps. Therefore, such experimental phenomena can be attributed to the optimal choice of the relative phase of two-color component involved in the broad-band OPA output. The advantage of the present two-hump scheme over the traditional two-color field scheme based on the superposition of two laser pulses, lies in that no optical delay line for the two pulses is required and therefore the timing jitter due to the pointing instability and vibration is removed. We should emphasize here that the observation of the phenomenon is strongly dependent on the broad bandwidth and the large two-hump distance of the OPA output spectrum.

In order to theoretically interpret our experimental results, we simulate the harmonic emission using the simplified Lewenstein model^[9,24,25] in the configuration of the two-color laser field. The time delay between the two fields is optimized in order to observe the harmonic spectrum varying from the discrete to the continuous. Note that the change of the time delay in the temporal domain is equivalent to the change of the relative

phase of the two-color field in the spectral domain. The two-color spectrum used in the simulation and their contribution to the harmonic emission are shown in Fig. 4. Figure 4(a) simulates the distance of two spectrum components is narrower than the one shown in Fig. 4(c). The differences between the time delay 1 and delay 2 are within 0.1 fs, due to the slight variations of the experimental chirps. One can see from the Figs. 2(b) and (d) that the harmonic emissions can vary from the discrete (red line) to the continuous (blue line) upon the variation of the delay value. The comparison of Figs. 4(a), (b) and (c), (d) shows the larger two-hump distance supports the larger degree of variation of the harmonic structure from the discrete to the continuous, which is agreement with our experimental result.

In conclusion, we experimentally investigate the relationship between the structure of the driving OPA spectrum and the shape of the generated high harmonic spectrum. It is found that the HHG exhibits more continuous spectrum upon broadening the OPA spectrum or introducing another weak spectrum component by tuning the OPA system. The generation of the XUV continuum using such broadband two-hump pulse produced by the optimal pump chirp is also experimentally demonstrated. It can be interpreted by the superposition effect of the two-color component of the OPA output. Therefore, the search of the optimal condition for the two-color component configuration through tuning the chirp of OPA pump pulse represents a simple scheme for the generation of the XUV continuum with photon energy exceeding 110 eV.

This work was supported by the National Natural Science Foundation of China (Nos. 11127901, 60921004, 11134010, 11222439, and 61108012), the National "973" Program of China (No. 2011CB808103), the Postdoctoral Science Foundation of China (Nos. 2012T50420 and 2012M520941), and the Postdoctoral Scientific Research Program of Shanghai (No. 12R21416600).

References

1. P. B. Corkum and F. Krausz, *Nature Phys.* **3**, 381 (2007).
2. Y. Zheng, Z. Zeng, P. Zou, L. Zhang, X. Li, P. Liu, R. Li, and Z. Xu, *Phys. Rev. Lett.* **103**, 043904 (2009).
3. J. Yao, Y. Li, and Y. Cheng, *Chin. Opt. Lett.* **09**, 041901 (2011).
4. Y. Zheng, H. Xiong, Z. Zeng, Y. Huo, Z. Wang, X. Ge, R. Li, and Z. Xu, *Chin. Opt. Lett.* **05**, S118 (2007).
5. K. Miyazaki, G. Miyaji, M. Kaku, and K. Yoshii, *Chin. Opt. Lett.* **5**, S139 (2007).
6. K. Zhao, Q. Zhang, M. Chini, Y. Wu, X. Wang, and Z. Chang, *Opt. Lett.* **37**, 3891 (2012).
7. M. Mohebbi and S. Batebi, *Chin. Opt. Lett.* **10**, 081901 (2012).
8. P. B. Corkum, *Phys. Rev. Lett.* **71**, 1994 (1993).
9. M. Lewenstein, Ph. Balcou, M. Yu. Ivanov, A. L'Huillier, and P. B. Corkum, *Phys. Rev. A* **49**, 2117 (1994).
10. P. Salières, B. Carré, L. Le Déroff, F. Grasbon, G. G. Paulus, H. Walther, R. Kopold, W. Becker, D. B. Milošević, A. Sanpera, and M. Lewenstein, *Science* **292**, 902 (2001).
11. V. S. Yakovlev, M. Ivanov, and F. Krausz, *Opt. Express* **15**, 15351 (2007).

12. P. Lan, E. J. Takahashi, and K. Midorikawa, *Phys. Rev. A* **81**, 061802 (2010).
13. L. Brugnera, F. Frank, D. J. Hoffmann, R. Torres, T. Siegel, J. G. Underwood, E. Springate, C. Froud, E. I. C. Turcu, J. W. G. Tisch, and J. P. Marangos, *Opt. Lett.* **35**, 3994 (2010).
14. D. Shafir, Y. Mairesse, D. M. Villeneuve, P. B. Corkum, and N. Dudovich, *Nature Phys.* **5**, 412 (2009).
15. P. Wei, C. Liu, C. Zhang, Y. Huang, Y. Leng, P. Liu, Y. Zheng, Z. Zeng, R. Li, and Z. Xu, *Opt. Express* **18**, 11664 (2010).
16. H. Niikura, H. J. Wörner, D. M. Villeneuve, and P. B. Corkum, *Phys. Rev. Lett.* **107**, 093004 (2011).
17. C. Vozzi, F. Calegari, F. Frassetto, L. Poletto, G. Sansone, P. Villoresi, M. Nisoli, S. De Silvestri, and S. Stagira, *Phys. Rev. A* **79**, 033842 (2009).
18. E. J. Takahashi, P. Lan, O. D. Mücke, Y. Nabekawa, and K. Midorikawa, *Phys. Rev. Lett.* **104**, 233901 (2010).
19. M. Negro, C. Vozzi, K. Kovacs, C. Altucci, R. Velotta, F. Frassetto, L. Poletto, P. Villoresi, S. De Silvestri, V. Tosa, and S. Stagira, *Laser Phys. Lett.* **8**, 875 (2011).
20. C. Zhang, P. Wei, Y. Huang, Y. Leng, Y. Zheng, Z. Zeng, R. Li, and Z. Xu, *Opt. Lett.* **34**, 2730 (2009).
21. Y. Xu, J. Wang, Y. Huang, Y. Li, X. Ln, and Y. Leng, *High Power Laser Sci. Eng.* **1**, 98 (2013).
22. C. Xu, C. Li, L. Song, D. Wang, and Y. Leng, *Chin. Opt. Lett.* **10**, 123202 (2012).
23. J. Zhang and D. S. Guo, *Phys. Rev. Lett.* **110**, 063002 (2013).
24. C. Liu, Y. Zheng, Z. Zeng, Ruxin Li, and Z. Xu, *Phys. Rev. A* **79**, 043826 (2009).
25. C. Liu, Y. Zheng, Z. Zeng, P. Liu, R. Li, and Z. Xu, *Opt. Express* **17**, 10319 (2009).